



Inorganic-organic hybrid pigments based on carminic acid and clay minerals

Graycyellê R.S. Cavalcanti, Francisco Rodrigues, Guanzheng Zhuang, Sebastien Balme, Jean-Marc Janot, Maria G Fonseca, Maguy Jaber

► To cite this version:

Graycyellê R.S. Cavalcanti, Francisco Rodrigues, Guanzheng Zhuang, Sebastien Balme, Jean-Marc Janot, et al.. Inorganic-organic hybrid pigments based on carminic acid and clay minerals. *Dyes and Pigments*, 2021, 190, pp.109306. 10.1016/j.dyepig.2021.109306 . hal-03236376

HAL Id: hal-03236376

<https://hal.sorbonne-universite.fr/hal-03236376>

Submitted on 26 May 2021

HAL is a multi-disciplinary open access archive for the deposit and dissemination of scientific research documents, whether they are published or not. The documents may come from teaching and research institutions in France or abroad, or from public or private research centers.

L'archive ouverte pluridisciplinaire **HAL**, est destinée au dépôt et à la diffusion de documents scientifiques de niveau recherche, publiés ou non, émanant des établissements d'enseignement et de recherche français ou étrangers, des laboratoires publics ou privés.

Inorganic-organic hybrid pigments based on carminic acid and clay minerals

Graycyellê R. S. Cavalcanti^{1,2}, Francisco Rodrigues^{2,3}, Guanzheng Zhuang^{1,4}, Sebastien Balme⁵, Jean-Marc Janot⁵, Maria G. Fonseca² and Maguy Jaber*¹

¹*Sorbonne Université, LAMS, CNRS UMR8220, Institut Universitaire de France, 75005 Paris, France*

²*LACOM, Paraíba Federal University – UFPB, João Pessoa, Paraíba, 58033-455, Brazil*

³*LabSAMA, Paraíba State University - UEPB, Campina Grande, Paraíba, 58109-790, Brazil*

⁴*China University of Geosciences, Beijing 100083, PR China*

⁵*Institut Européen des Membranes, UMR5635 UM ENCSM CNRS, Place Eugène Bataillon, 34095 Montpellier cedex 5, France*

Highlights

- New hybrid pigments based on carminic acid and clay minerals were prepared.
- The interactions at the molecular level were highlighted.
- The prepared pigments from hydrogels presented high stability under visible light.
- Coating with organosilanes may act as a protective layer for the pigments face to light exposure.

Abstract

Hybrid pigments based on carminic acid (CA) stabilized by clay minerals have been prepared. Three different pathways were used: CA@saponite; CA@Al-pillared saponite; and hydrogels of saponite-CA or montmorillonite-CA covered by polyorganosilane (POS). Pigments were characterized by a set of different techniques including X-Ray diffraction (XRD), transmission electron microscopy (TEM), infrared spectroscopy (FTIR), solid state nuclear magnetic resonance (NMR) and time-resolved fluorescence (TRF) spectroscopies. The color parameters, i.e., $L^*a^*b^*$, were measured. In addition, the photostability of the samples under visible light was evaluated. The results showed that CA@PilSap presented a greater stability compared to CA@Saponite. The pigments obtained from hydrogels presented the greatest light stability due to the coverage with POS that acts as a protective layer.

Keywords: hybrid pigments; saponite; carminic acid; photodegradation

1. Introduction

The use of pigments from natural origins has been reported since ancient times for various purposes such as paints, cosmetics, dyeing textiles and coloring foods [1,2]. Dyes derived from *coccid* insects are commonly used and constitute one of the most known and exploited classes of red organic dyes at the present day [3].

Carminic acid (CA), (IUPAC nomenclature 17-C- α -glucopyranosyl-3,5,6,8-tetrahydroxy-1-methyl-2-anthraquinone), has been reported as the main derivative dye from cochineal with a high yield of extraction [2–4]. CA is vulnerable to thermal variations and photodegradation when used in its pure form. This phenomenon is commonly observed in paintings and promotes the increase of studies related to both the photodegradation mechanisms and the development of new stable pigments derived from CA [5,6].

The increase in system stability has been innumerable times related to the preparation of pigments involving inorganic matrices. Studies have shown that the synergy of organic and inorganic compounds in hybrid materials may form new materials with enhanced properties [4,7-9]. In the case of pigments, greater stability can be improved by the formation of organic-inorganic hybrid pigments.

The development of pigments based on inorganic substrates and organic compounds, is not a recent issue. Maya blue, composed of palygorskite and indigo dye, is a famous archeological example of organic-inorganic hybrid pigment. It was widely used in paintings, murals and ceramics from the Mayan civilization [7,8]. Its incredible stability against acid, alkaline and organic corrosion and degradation over time has recently attracted much interest in the fields of materials, chemistry and archeology [4,9].

Although the real nature of Maya blue is controversial, it is believed that the unique clay-dye interaction between palygorskite and indigo endows its remarkable stability. Maya blue encourages that clay-dye hybrid pigments may be a promising way to develop new durable

hybrid pigments. In general, clay minerals have specific physicochemical properties such as adsorption, cation exchange capacity, swelling capacity, ability to form colloidal solutions, optimum rheological behavior and dispersibility in water; which have allowed them to be used in different ways in various applications [10,11]. In addition, studies with other clay minerals allow research about the impact of the structure and layer loading on the coordination of metallic ions, as well as the capacity of interactions with positively charged species such as cationic dyes [12,13].

Recently, other clay minerals have been used as an inorganic matrix to prepare hybrid pigments such as saponite [14,15], montmorillonite [6,16], palygorskite [8,17], sepiolite [7,18] and halloysite [19], etc. Montmorillonite (Mt) and saponite (Sap) are phyllosilicates belonging to the smectite group. The structural variability, as well as the possibility of modifying the clay minerals belonging to this group, allows different interactions with dyes that vary according to the structural composition [19, 20].

The interaction of dye molecules with clay minerals is the key parameter to prepare inorganic-organic hybrid solids that are more stable than the dyes in their isolated form [11,22].

Although they are excellent adsorbents for different organic molecules, clay minerals present limitations in relation to the species that can be adsorbed. Therefore, some modifications have been proposed to overcome these limitations [23,24]. The main clay modifications reported in the literature are ion exchange [25], intercalation of cationic surfactants [26], pillaring with different metal oxides [27], silylation [28], coating of hexadecyltrimethoxysilane (HDTMS) and tetraethoxysilane (TEOS) [29].

In this context, the present work intended to synthesize new stable pigments based on CA and clay minerals. Three different pathways were used: direct adsorption of CA on raw synthetic saponite; adsorption of CA on Al-pillared saponite; and hydrothermal treatment of CA with hydrogels of saponite and montmorillonite followed by covering with polyorganosilane

(POS). The prepared pigments were characterized, and their chemical and light stabilities were evaluated.

2. Experimental

All chemicals were analytical grade and were used without additional purification. In Table SM1 are summarized the list of samples and methods used in the synthesis.

2.1 Synthesis of saponite (*Sap*)

Synthetic saponite was prepared from the reagent mixture, added in the following order: deionized water (65.38 g, 3.63 mol), hydrofluoric acid (0.38 g, 0.95 mmol, 40% w/w; Fluka), sodium acetate (0.18 g, 2.15 mmol, 99%; Sigma-Aldrich), magnesium acetate (3.46 g, 16.2 mmol, 99%, Sigma-Aldrich), alumina (0.34 g, 3.33 mmol, 99.8%; Sigma-Aldrich) and silica (1.15 g, 19.14 mmol, Aerosil 380; 99.8%; DEGU). The hydrogels were prepared with the mol composition of $\text{Na}_{0.4}[(\text{Si}_{3.6}\text{Al}_{0.3})\text{Mg}_3\text{O}_{10}(\text{OH},\text{F})_2]$, aged for 4 h at room temperature under magnetic stirring and then was autoclaved at 220 °C for 72 h. The autoclaves were cooled to room temperature and the product were washed with deionized water and centrifuged for 7 to 10 times [30].

2.2 Pillaring process of saponite (*PilSap*)

The preparation of Al-pillared saponite followed the procedure adapted from Bergaoui *et al.* (1995) [31]. First, the pillaring agent was obtained by hydrolysis of aluminum chloride (1.6 g, 12 mmol Al 99%; Sigma-Aldrich) with a NaOH (1.01 g, 26.4 mmol OH, 98.9%; Merck) solution up to 2.2 OH:Al ratio and final concentration of 0.1 mol L⁻¹. The reactional mixture was aged for 24 h at room temperature (~25 °C) under magnetic stirring. Meanwhile, the suspension (7.5 mmol Al³⁺ g⁻¹ clay) containing saponite (1.6 g) was prepared by suspending the clay in water (500 mL) and aged for 3 h at the same conditions. Later, aluminum pillaring solution (120 mL) was added dropwise (~0.5 mL min⁻¹) to a clay suspension and was

maintained under magnetic stirring for 24 h at room temperature. The obtained solid (Sap-Al) was centrifuged at 8000 rpm for 20 min and washed with deionized water and dried at 50 °C for 24 h. After that, sample was calcined up to 500 °C for 2 h and then denoted PilSap.

2.3 Preparation of hybrid pigments

2.3.1 Adsorption procedure

Saponite and Al-pillared saponite samples were loaded with carminic acid (CA; 99%; Sigma-Aldrich, pKa values of 2.8, 5.4 and 8.1): for each sample, a clay amount (300 mg) was suspended in an aqueous solution of carminic acid (100 mL, 0.6 g L⁻¹) and was left under stirring for 4 h at room temperature (~25 °C) under magnetic stirring. The pH of the solution was adjusted to 2.5, which is the pH where CA species are neutral. The samples were then centrifuged, washed with deionized water and dried at 50 °C for 24 h, following the same method previously described [6].

2.3.2 Pigments synthesis from clay hydrogels

The hydrogels were prepared with the mol composition of Na_{0.4}[(Si_{3.6}Al_{0.3}) Mg₃O₁₀(OH,F)₂] and Na_{0.4}[(Si₄)(Al_{1.6}Mg_{0.4})O₁₀(OH,F)₂], for saponite and montmorillonite precursors, respectively. The amounts of used salts are described in the Table SM2. The mixtures were maintained under stirring at room temperature for 48 h at pH 5. Then, the respective hydrogels (12 g) and carminic acid (1.2 g, 10% m/m) were autoclaved at 120 °C for 10 days. After that, the autoclaves were cooled to room temperature and the final product were washed with deionized water (~ 150 mL) and centrifuged and dried at 50 °C for 48 h. Saponite and

montmorillonite precursors samples obtained by coprecipitation were named CA-precSap-120 and CA-precMt-120, respectively.

2.3.3 Coating with TEOS / HDTMS

Coating method followed methodology described by Zhuang *et al.* 2019 [19]. First, CA-precSap-120 or CA-precMt-120 (200 mg) was dispersed in ammonia (25%; Sigma-Aldrich) saturated in ethanol (95%; VWR) solution (10 mL) prepared in 9:1 volume/volume proportion. Suspension was maintained under magnetic stirring for 5 min. Then, TEOS (99%; Sigma-Aldrich) (0.32 mL, 0.15 mmol) and HDTMS (85%; Sigma-Aldrich) (0.546 mL, 0.15 mmol) were added into the mixture that was ultrasonicated at 50 °C for 30 min. Finally, deionized water (1.44 mL) was quickly injected into the solution that was maintained under same conditions for 1 h. The samples after coating were denominated CA@Sap-Si, CA-precSap-120-Si and CA-precMt-120-Si.

2.4 Desorption study

Desorption experiments were performed by dispersing the pigments (10 mg) in deionized water (10 mL) under magnetic stirring at room temperature for 20 min. Then, the solids were centrifuged at 10.000 rpm for 5 min. Finally, the amount of dye remaining in the supernatant was determined by UV-Vis molecular absorption spectroscopy with an Ocean Optics device with halogen light source and deuterium HL-2000-FHSA operating in the 200-900 nm range. The supernatants were placed in quartz tubes with accessories for liquids containing 1 cm optical path. The concentration of carminic acid in solution was quantified at 485 nm in the

range of 2 to 50 mg L⁻¹ and the amount of dye (q_e) in the supernatant after desorption was determined according to Equation 1

$$q_e = \frac{(C_e)V}{m} \quad (1)$$

where C_e (mg L⁻¹) are the concentrations of the dye after desorption, m (mg) mass of clay and V (L) the volume of deionized water.

3. Characterizations

3.1 X-ray diffraction (XRD)

X-ray diffractograms were recorded using the D8 Advance Bruker-AXS X-ray diffractometer with 30 kV voltage and 30 mA current and CuK α radiation ($\lambda = 1.5405 \text{ \AA}$). The XRD patterns were obtained between (2θ) of 5 to 80 ° with a scan rate of 0.5 degrees min⁻¹.

Sap, Sap-Al and PilSap samples required an additional procedure to obtain higher quality diffractograms. Thus, the solid (200 mg) was dispersed in water (2 mL) and was kept under magnetic stirring until a homogeneous dispersion. Subsequently the mixture was deposited onto a glass slide to form a homogeneous layer. The slices were dried at 50 °C for 24 h and resulted in a film formation. The diffractograms were then collected under the same conditions as for the other samples.

3.2 ATR-FTIR

Infrared analyzes were performed on the Agilent Cary 630 FTIR spectrometer using the Attenuated Total Reflectance mode (ATR) with a diamond crystal detector and the spectral resolution of 2 cm⁻¹ and 30 accumulation scans. The spectra were collected by the Microlab FTIR Software (Agilent Technologies) between 4000 and 600 cm⁻¹.

3.3 Thermal analysis (TG/DTG)

Thermogravimetric analyses were performed using a TA Instrument SDT Q600 analyzer with a heating rate of 5 °C min⁻¹ from 25 °C to 900 °C, under dry air flow of 10 mL min⁻¹ and using an alumina crucible.

3.4 Solid state nuclear magnetic resonance (¹³C CP-MAS- and ²⁷Al MAS-NMR)

The ²⁷Al NMR spectra were obtained on a Bruker Avance III spectrometer equipped with a 4 mm HX MAS probe, operating at a frequency of 130.33 MHz. Al (NO₃)₃ (0 ppm) was used as an external standard. ¹³C spectra were obtained on a Bruker Avance 500 spectrometer operating at a frequency of 60.37 MHz. Cross-polarization of protons (CP-MAS) was applied with a contact time of 1 ms. The samples were rotated at the magic angle at a frequency of 10 kHz. The pulse length of ¹³C was 5 ms (close to $\pi/2$) and the recycling delay was 3 s.

3.5 Transmission electron microscopy (TEM)

Transmission electron microscopy analyzes were performed under a JEOL 2010 microscope operating at 200 kV LaB6. To prepare the sample a few milligrams of the sample are mixed in a Beem capsule with Agar 100 embedding resin. After polymerization at 60°C overnight, the blocks are cut using a microtome equipped with a diamond knife. The ultra-thin slices about 50 nm, are recovered on copper grids and examined. The micrography were treated using Gatan Software.

3.6 Contact angle analysis

The evaluation of the hydrophobicity of the pigments was performed from the preparation of pellets of 5 mm diameter in which a drop of 10 µl of water was added to calculate the angle

generated between the plane tangent to the surface of the material on which the drop was deposited [8,32]. Adobe Photoshop software was used for the treatment of images.

3.7 Time-resolved fluorescence

The fluorescence lifetimes were obtained by the time-correlated single-photon counting technique. The fluorescence decay of CA and CA loaded in different materials were directly performed on powder deposited on a cover slide. The excitation wavelength was achieved by using a SuperK Extrem high power white supercontinuum laser (NTK Photonics, model EXR-15) as a continuum pulsed source. The wavelength ($\lambda=580$ nm) was selected by coupling to a monochromator (Jobin–Yvon H10). The repetition rate was set to 38.9 MHz; the excitation pulse duration on this device is around 6 ps (full-width-at-half-maximum, FWHM). The emission of fluorescence is collected using a parabolic mirror and detected, after passing through a polarizer oriented at the magic angle (54.73°) to polarization of excitation, through a double monochromator ($\lambda=660$ nm) Jobin–Yvon DH10 on a hybrid PMT detector HPM-100-40 (Becker & Hickl). The instrumental response function of the equipment was measured by using a dilute suspension of polystyrene nanospheres in water (70 nm of diameter) as a scattering solution; it was typically about 130-160 ps FWHM. Decays were collected at a maximum count rate of 15 kHz into 4096 channels using an acquisition card SPC-730(Becker & Hickl). The time per channel was set around 6 ps ch⁻¹ in order to fit a full decay in the experimental time window. All decays were collected to have at least 1.5 and 10⁶ counts in total. Decay analysis was performed using a Levenberg–Marquardt algorithm. The fluorescence decay and anisotropy function were analyzed as a sum of exponential as

$$I(t) = \sum_{i=1}^n a_i e^{(-t/\tau_i)} \quad (2)$$

Where $I(t)$ is the fluorescence intensity, a_i a pre-exponential factor, τ_i the fluorescence lifetime, Fluorescence lifetimes were calculated from data collected at magic angle by iterative adjustment after convolution of a pump profile (scattered light). We assumed a Poisson distribution of counts in the calculation of the χ^2 criterion; residuals profiles and autocorrelation function as well as Durbin-Watson and skewness factor were used in order to estimate the quality of the adjustment. The number of exponentials used for the fit was increased until all the statistical criterions were improved.

3.8 Light-induced aging and diffuse reflectance UV-Vis

Light-induced tests were performed by exposure of the solid pigments face to white light irradiation for 354 h, using an LED lamp set to provide 66 Klx of illumination intensity. Photostability were evaluated over time by means of spectrophotometric measurements in triplicate by using an Ocean Optics device with light source of halogen and deuterium HL-2000-FHSA and incident light beam, with acquisition from the Ocean detector Optics USB4000. For each acquisition, an average of 30 scans were used under a wavelength range of 400 to 950 nm. The CIELAB data were calculated according to the “Commission Internationale of l’Eclairage” (CIE). The L^* , a^* and b^* coordinates were obtained for the ΔE^* determination, which refers to changes in the pigment color over time of exposure to light. The total color difference (ΔE^*) was obtained from Equation 3:

$$\left((a_{*i+j} - a_{*i})^2 + (b_{*i+j} - b_{*i})^2 + (L_{*i+j} - L_{*i})^2 \right)^{1/2} \quad (3)$$

where, i and j refer to the number of measurements taken over time.

The reflectance spectra before and after exposure to light were also recorded for the samples of the pigments under the same conditions as described previously.

4. Results and discussions

4.1 X-ray diffraction (XRD)

XRD patterns for the saponite samples are presented in Figure 1i and showed the presence of characteristic clay mineral reflections. In particular, the reflection at 60.6° with a distance of 0.153 nm (060) suggested the formation of a trioctahedral structure. Other reflections at 19.7° , 27.8° , 34.9° and 53.2° are also characteristic of saponite [33,34]. For all samples the reflection in the 001 plane were enlarged or very weak, which is associated with the loss of periodicity along direction c and indicates disordered lamellar stacking [35]. Therefore, at low angles (Figure 1ii), oriented films were prepared as described in the experimental section and allow a better visualization of the (001) reflection of the saponite at $2\theta = 7.34$ with a d_{001} value = 1.21 nm, [36]. Therefore, basal spacing increased to 1.42 and 1.37 nm for Sap-Al and PilSap samples and suggested the intercalation of Keggin ion and the pillarization of the saponite after calcination [23,31,32].

After interaction with carminic acid (Figure 1iii), the (001) reflection plane presented a better definition. The increase in the basal spacing value from 1.21 to 1.54 nm in CA@Sap and from 1.37 to 1.5 nm in CA@PilSap also suggested the intercalation of the dye in the interlayer space of the saponite.

Concerning the XRD patterns of the dried samples obtained from hydrogels, any reflection of the saponite and montmorillonite was not observed (see Figure SM1).

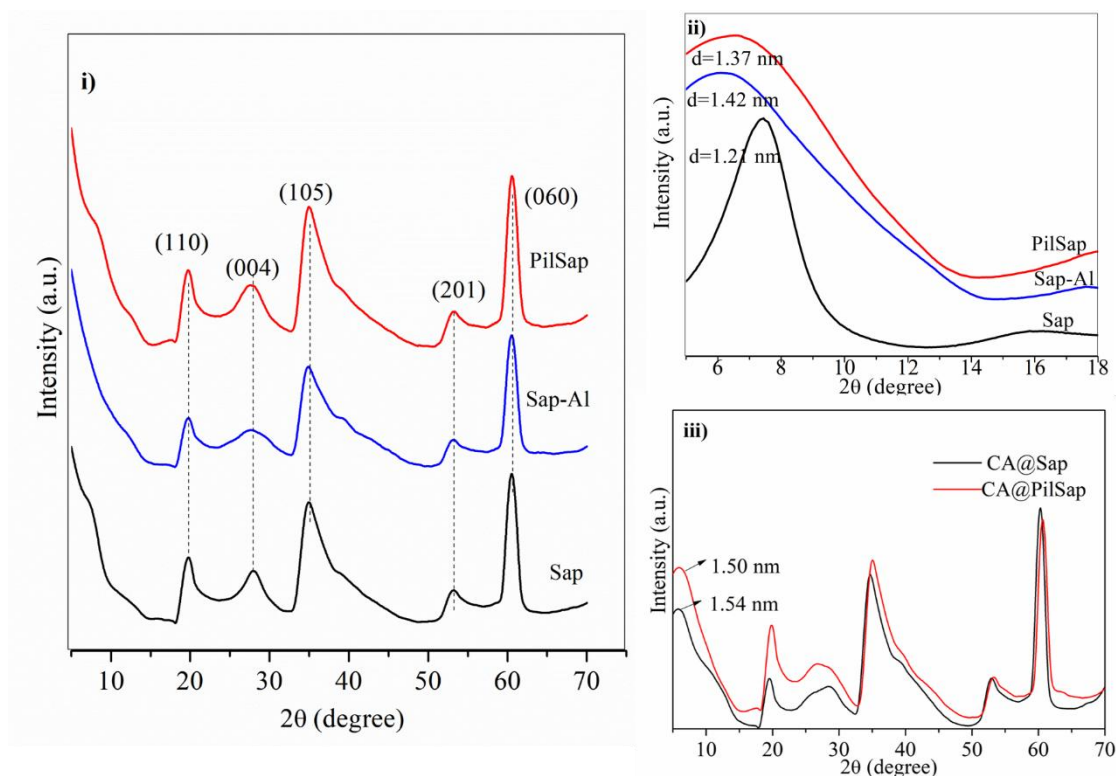


Figure 1 - X-ray diffractograms of (i) saponite and modified saponite before dye adsorption between 8 and 70 ° (2θ) ii) saponite and modified saponite before dye adsorption between 2 and 20 ° (2θ) and iii) CA@Sap and CA@PilSap hybrids.

4.2 Infrared Spectroscopy (ATR-FTIR)

Infrared spectroscopy was performed on samples before and after adsorption of carminic acid, aiming to identify the presence of the CA in the samples and the nature of the dye/clay minerals interactions. The structure and spectrum of carminic acid are presented in Figure 2i-iii. The band at 1710 cm^{-1} was assigned to C=O stretching of the carboxylic acid present in the molecule [39]. The bands observed at 1611 , 1566 , and 1426 cm^{-1} were attributed to quinone C=O stretching vibrations; C=C stretching and OH deformation, respectively [40].

For saponite and pillared saponite, characteristic bands of the clay mineral were observed: band around 3684 cm^{-1} corresponds to the structural -OH stretching and the wide band around 982 cm^{-1} is attributed to the Si-O-Si stretching of the saponite structure [41].

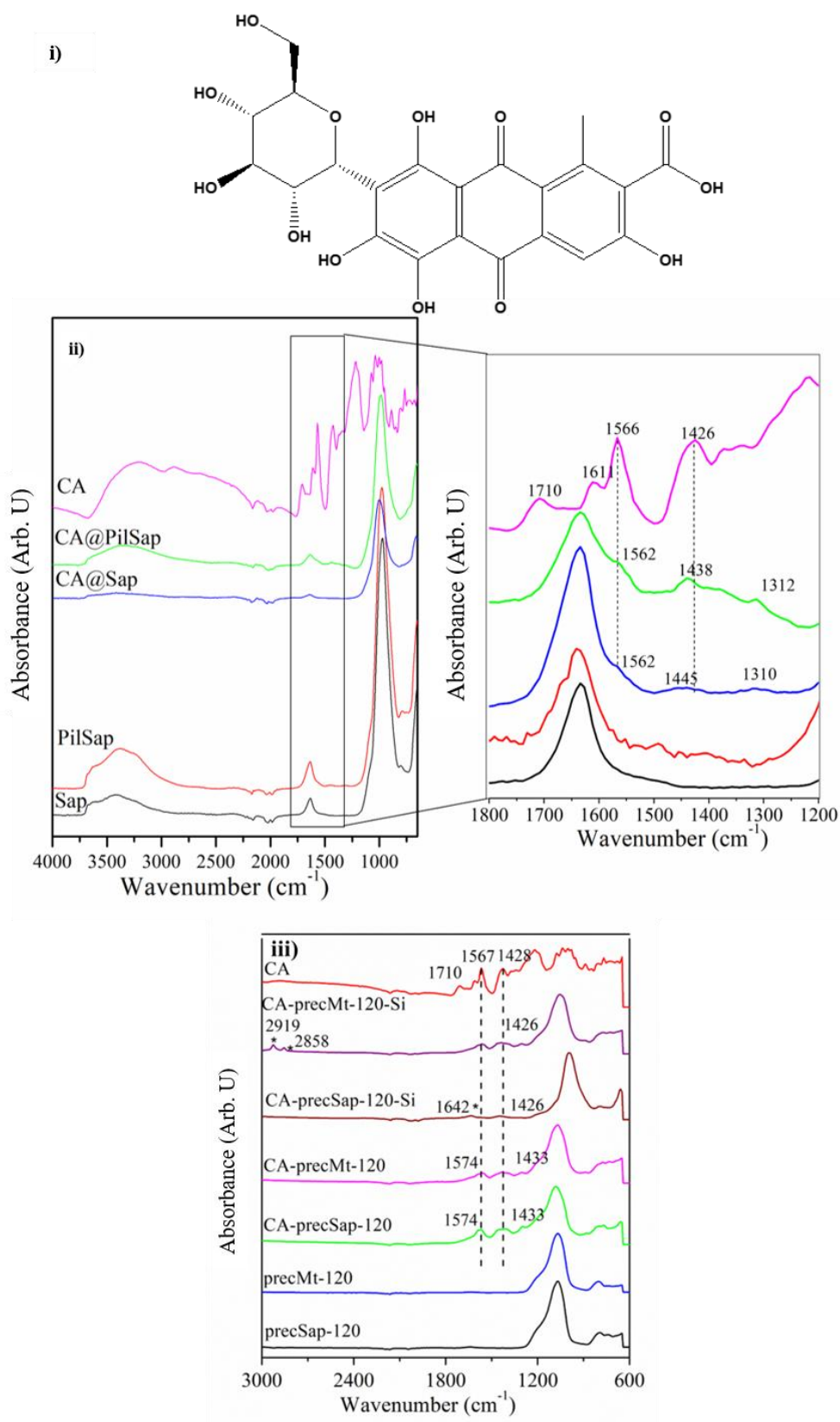
After CA sorption on Sap and PilSap, C=O stretching was not observed, suggesting that the interaction between the dye and the inorganic part occurred mainly via this function [39]. C=C stretching did not show significant variation and is observed at 1562 cm^{-1} for both clay samples. In contrast, the OH deformation shifted from 1426 to 1445 cm^{-1} in CA@Sap and to 1438 cm^{-1} in CA@PilSap. This can also be due to an interaction between the catechol groups of the dye and the clay mineral.

In the samples heated at $120\text{ }^{\circ}\text{C}$ without carminic acid, the spectra did not present characteristic bands of the clay mineral structure. However, the band around 982 cm^{-1} can be assigned to the Si-OH stretching and formation of silicate in the clay hydrogels. (Figure 2iii). This may also indicate a poor crystallization of the saponite and montmorillonite precursors, which is in agreement with the XRD results [42].

Regarding samples obtained in the presence of CA and heated at 120°C , the presence of bands assigned to C=C stretching at 1567 cm^{-1} and OH deformation at 1419 cm^{-1} in both materials were associated to the anthraquinone functions that shifted compared to the one in the free carminic acid. This is due to the interaction between the dye and the oxide mixture present in the gels and suggests coordination between quinone and metal cations in the mixture, as well as the sorption of carminic acid on the oxide surface.

For both CA coated samples, the same bands than in the spectra of the uncoated solids were observed. However, the band at 1426 cm^{-1} which is attributed to the -OH stretching in the anthraquinone appeared unchanged, which may be related to the migration of the dye molecules to the surface of the solids. The coating of the CA-precMt-120-Si was evidenced by the presence of the bands at 2910 cm^{-1} and 2858 cm^{-1} assigned to asymmetric and

331 symmetric CH stretchings and the band at 1642 cm^{-1} for CA-precSap-120-Si assigned to
 332 hexadecyl group [43] .



333

Figure 2 – i) Structure of the carminic acid and infrared spectra of ii) initial samples and hybrid pigments and iii) initial samples and hybrid pigments obtained by coprecipitation. (*) TEOS/HDTMS signals.

4.3 Thermogravimetric analysis (TGA)

TG (Figure SM2) and DTG (Figure 3i) curves for Sap and PilSap presented two mass loss steps. The first step was attributed to the adsorbed and interlayer water losses at $T_{\max} = 65\text{ }^{\circ}\text{C}$ and represented 8.6% for Sap and 5.4% for PilSap. The second event around 680-850 $^{\circ}\text{C}$ was attributed to the dehydroxylation of OH groups presented at the edges of the clay mineral layers and corresponded to 3.1% and 2.9% for pillared saponite and saponite, respectively. [44]. Free dye begins its degradation at 162 $^{\circ}\text{C}$ (Figure SM2). Samples CA@Sap and CA@PilSap loaded with carminic acid, presented two events of mass loss. Organic matter decomposition and dehydration occurred simultaneously in 32-164 $^{\circ}\text{C}$ and 35-200 $^{\circ}\text{C}$ and was associated to mass loss of 13.2% and 11.9% for CA@Sap and CA@PilSap, respectively. The last event between 700-800 $^{\circ}\text{C}$ referred to the clay mineral dehydroxylation for both samples. These results suggested that CA adsorbed in Al-pillaring clay presented higher thermal stability than free CA [6,16].

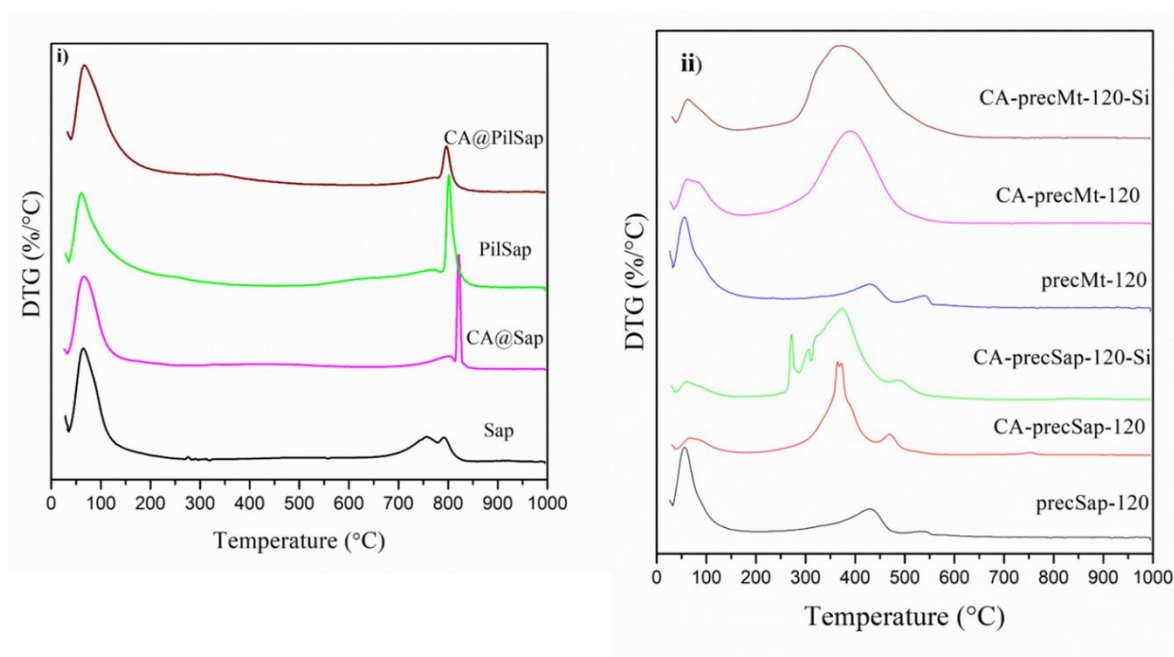


Figure 3 - DTG curves for i) references samples and hybrid pigments obtained by adsorption
ii) references samples and hybrid pigments obtained by coprecipitation.

The DTG curves of precMt-120, CA-Mt-120 and CA-precMt-120-Si (Figure 3ii) presented two mass loss steps: the first one at about 40-160 °C with mass losses of 4.87%, 10.12% and 6.82% were attributed to dehydration (loss of physisorbed water). DTG curves of precSap-120, CA-precSap-120 and CA-precSap-120-Si presented three distinct profiles with mass loss in two, three and four events, respectively. The higher mass loss (48%) obtained at 280 °C indicated that the dye degraded at higher temperatures compared to its isolated form (162°C) due probably to a strong interaction with the inorganic matrix [45].

4.4 ^{27}Al and ^{13}C CP MAS solid state nuclear magnetic resonance

The ^{27}Al NMR spectra for the Sap and PilSap samples are shown in Figure 4i-ii. Both samples presented signals at 65.6 ppm due to the presence of structural tetrahedral aluminium [27,46,47]. However, PilSap exhibited two new signals at 6.37 and 33.4 ppm, that were

attributed to hexa- and penta-coordinated Al, respectively. The high intensity signal refers to hexacoordinated aluminium (^{VI}Al) in the pillars. The tetracoordinated aluminium (^{IV}Al) signals refer to a central overlap aluminium in the Keggin structure that comprises of 13 Al atoms with a tetrahedral Al-center atom surrounded by 12 octahedral Al atoms [48,49]. The obtained data suggested the successful formation of the aluminium pillars in the PilSap sample.

^{27}Al NMR spectra obtained for CA@Sap presented a similar profile to the one observed in Sap. Moreover, chemical shifts changed from 8.41 to 6.97 ppm in the signal attributed to ^{VI}Al . This shift may suggest the interactions between CA and Si-OH-Al-OH in the Sap [6,16]. In contrast, the CA@PilSap spectrum showed a significant decrease in peak intensity at 33.4 ppm for penta-coordinated aluminium and was related to an interaction between the aluminium and the dye.

Hydrothermally treated samples exhibited similar ^{27}Al NMR spectra with an intense peak centered at 7.83 ppm attributed for hexacoordinated aluminium (^{VI}Al) and a signal at 54 ppm attributed to tetracoordinated aluminium (^{IV}Al) [50,51].

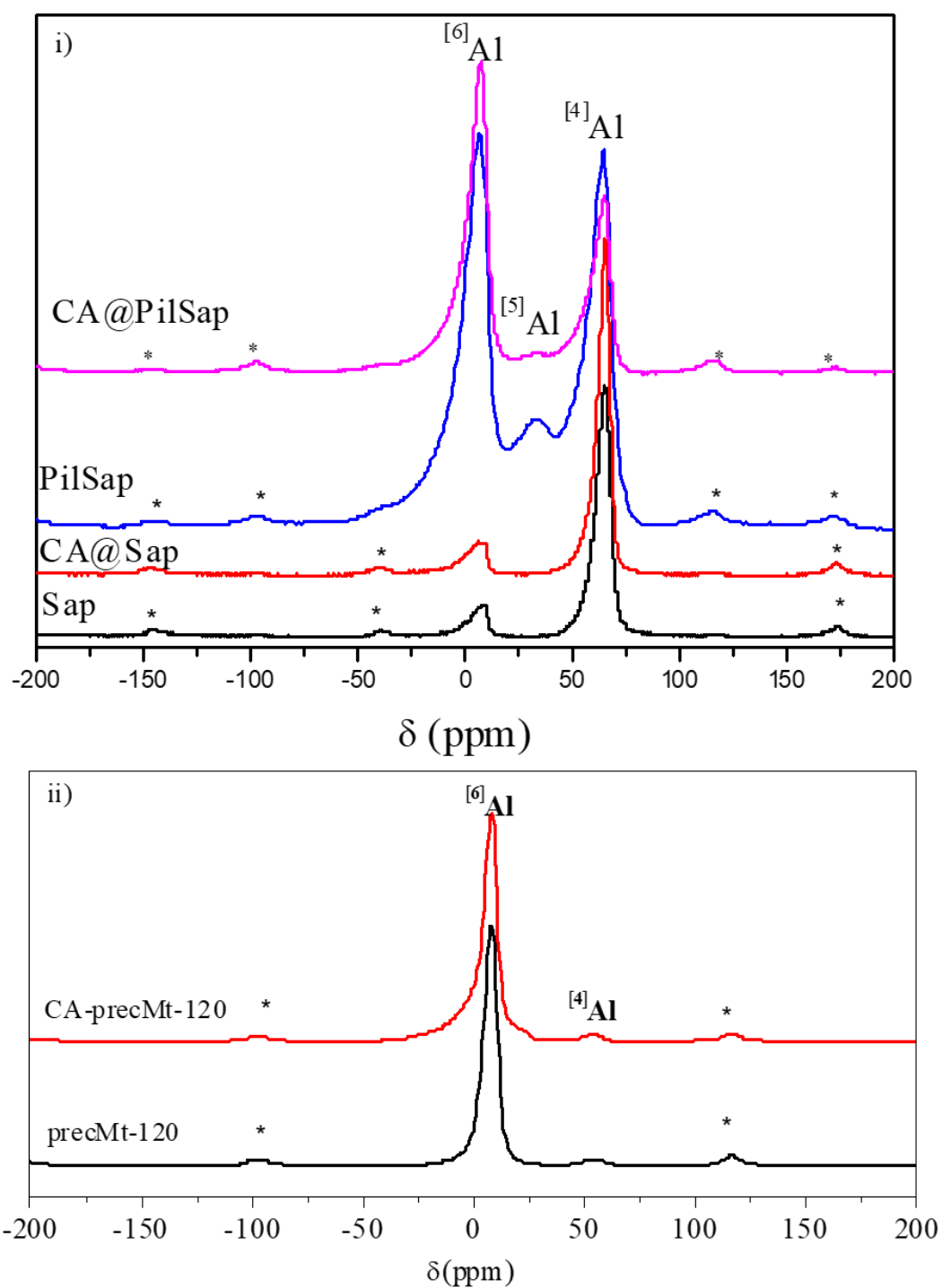


Figure 4- ^{27}Al NMR spectra of (i) precursor matrix and hybrid pigments obtained by adsorption, and (ii) precursor matrix and hybrid pigment obtained by coprecipitation, (*) Side spinning bands.

¹³C CP/MAS NMR spectra of carminic acid and the derived pigments are shown in Figure 5i-ii and the chemical shifts are also summarized in Table 1. Resonance spectral regions for anthraquinone structure were observed as described in the literature [6,16]. The 60-80 ppm region refers to the sugar moiety present in the molecule, while the 20.6 ppm peak is attributed to the methyl group on C-8. The signals at 185 and 171 ppm are related to the ketones and carboxylate functions, respectively. The spectrum of CA@Sap presented a similar profile to the one observed for the free dye, but some displacements were noted from 119 ppm to 113 ppm, from 112 ppm to 102 ppm and from 105 ppm to 100 ppm, attributed to C-2, C-4a,5 and C-8 atoms, respectively [4]. The shifts can be correlated to both the protection effect and the inductive effect through the carbon environments in the anthraquinone part of the dye after interaction between the OH groups of the C-2 and C-4 atoms with saponite. However, the region in the spectrum assigned to C-4 as well as C-1 and C-3 carbons are not well resolved to observe the chemical shifts.

Figure 5ii showed ¹³C CP/MAS NMR spectrum for CA-precMt-120-Si. Variations in the chemical shifts were also observed, from 119 ppm to 124 ppm, from 153 ppm to 149 ppm and from 20.6 ppm to 22.9 ppm, attributed to C-2, C-3 and C8 atoms, respectively. In the region of the C-9,10, the signal was changed from 185 to 182 ppm for CA-precMt-120, which suggests the chelation of the anthraquinone dye with the aluminum oxide dispersed in the gel. Similar results were obtained in previous work [4,6,16].

Table 1 - Main chemical shifts observed in the ¹³C CP/MAS NMR spectra for the CA@Sap and CA-precMt-120 samples.

Carbon	<i>Chemical shifts (ppm)</i>		
	CA	CA@Sap	CA-precMt-120
C-2	119	113	124
C-3	153	-	149
C-4a,5	112	102	-
C-8b	105	100	-
C-8	20.6	20.6	22.9
C-9,10	185	-	182

410

411

4.5 Transmission electron microscopy (TEM)

TEM micrographs (Figure 6) indicated that after hydrothermal synthesis, the samples did not present profiles characteristic of the smectites, which is in agreement with XRD analysis, that suggests the formation of solids with low crystallinity. Moreover, the CA-precMt-120 sample (Figure 6ii) presented layered structures in the gel but not uniform distribution. Presence of layered structures can promote additional stability to the pigment compared to CA-precSap-120 sample. The synthesis was performed at neutral pH and relatively low temperature, considering the thermal stability of the dye and its speciation.

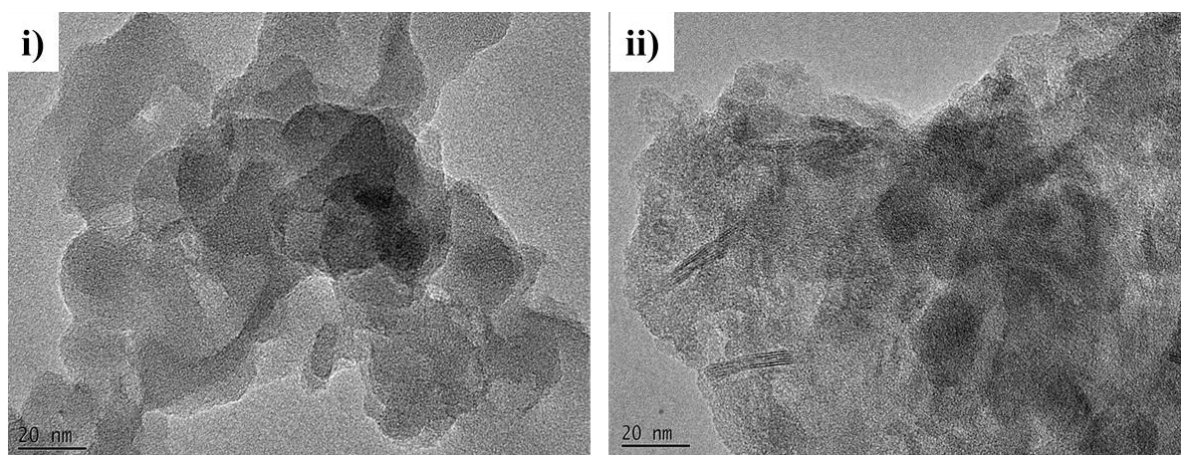


Figure 5- TEM images for i) CA-precSap-120 and ii) CA-precMt-120.

4.6 Time-resolved fluorescence

In previous works, the interaction of clay minerals with anthraquinone dyes has been observed providing results regarding the stability of the formed systems. [4,6,14,16]. As described by Fournier, F. *et al.* 2016 [4], the fluorescence property of carminic acid is entirely related to the environment in which it is inserted. Compared to our previous work, here the fluorescence lifetime was measured directly on the powder in order to be compared with the result obtained by the other techniques (NMR, XRD, FTIR). It results that the average

lifetime was found to be 0.052 ns while it is about 0.2 ns in water[16]. The fluorescence decay is well fitted by three components 0.492 ns, 0.107 ns and 0.025 ns where the main one is the shortest (71.52 %), as shown in Table 2. After co-precipitation on Mt and Sap, the mean lifetime decreases to 0.035 and 0.012 respectively. However, the long lifetime component increases from 0.49 ns to ~1 ns. This confirms the interaction between the CA and the inorganic precursor. However these interactions are weak since we could expect that the confinement will significantly increase the fluorescence lifetime as previously shown [4,16]. For the both clays, the introduction of HDTMS molecules increases the average lifetime that is only due to a lengthening of the long component and its yield. This could be assigned to a hydrophobic environment of the CA. Indeed, it was found that the length of carbon chain of primary alcohol increases the fluorescence lifetime of CA considering the same protonation state [54].

For the CA@PilSap, we can observe a significant lengthening of the main fluorescent lifetime (1.089 ns) compared to the CA-precSap-120. The long and average component has yield about 33 % each. This can be assigned to the presence of penta-coordinated aluminum that chelates the CA. In that case, the CA is stabilized.

Table 2- Fluorescence lifetime (τ_i) and average lifetime (τ_{av})

Samples	τ_1 (ns) / (yield)	τ_2 (ns) / (yield)	τ_3 (ns) / (yied)	τ_4 (ns) / (yied)	$\tau_{(av)}$ (ns)
CA	0.492 (1.29)	0.107 (27.19)	0.025 (71.52)	-	0.053
CA@PilSap	2.447 (34.29)	0.626 (33.47)	0.19 (18.41)	0.043 (13.82)	1.089
CA-precSap-120	0.923 (0.7)	0.204 (0.13)	0.004 (98.75)		0.012
CA-precSap-120-Si	1.542 (4.9)	0.198 (1.34)	0.003 (93.75)		0.081
CA-precMt-120	1.096 (2.57)	0.273 (1.9)	0.002 (95.53)		0.035
CA-precMt-120-Si	1.288 (6.99)	0.279 (3.61)	0.001 (89.4)		0.101

4.7 Desorption tests

Desorption tests performed on the samples containing carminic acid showed dye release in water, as can be seen in the spectra obtained in solution for CA@Sap, CA-precSap-120 and CA-precMt-120, Figure SM2. Maximum released amounts were 47, 65 and 70 mg L⁻¹, respectively. Aluminium-pillared, CA-precSap-120-Si and CA-precMt-120-Si sample did not present any desorption in water or ethanol.

4.8 Contact surface angle tests

A contact angle of 133.8 ° was obtained for CA-precSap-120-Si and 130.9 ° for CA-precMt-120-Si. Both samples have hydrophobic surfaces with contact angle values higher than 90°. Figure SM3 showed the pigment immiscibility in water.

4.9 Discussion

The results showed that the prepared pigments by adsorption presented different characteristics from those produced via hydrothermal treatment process. This fact is directly related to the speciation of carminic acid. The synthesis of CA@Sap and CA@PilSap was realized at pH 2.5 ($pK_{a1} = 2.8$). At that pH, the dye is mainly in its neutral form interacting directly or indirectly through water bridges with the exchangeable cations in the interlayer space. Moreover, some of the adsorbed CA molecules may involve hydrogen-bonds between the CO function and the water molecules that are present in the clay structure [55]. In the CA@PilSap sample, chelation occurs between the aluminium pillars and the dye promoting dye stabilization. as showed in the FTIR and ^{27}Al NMR results (Figure 6).

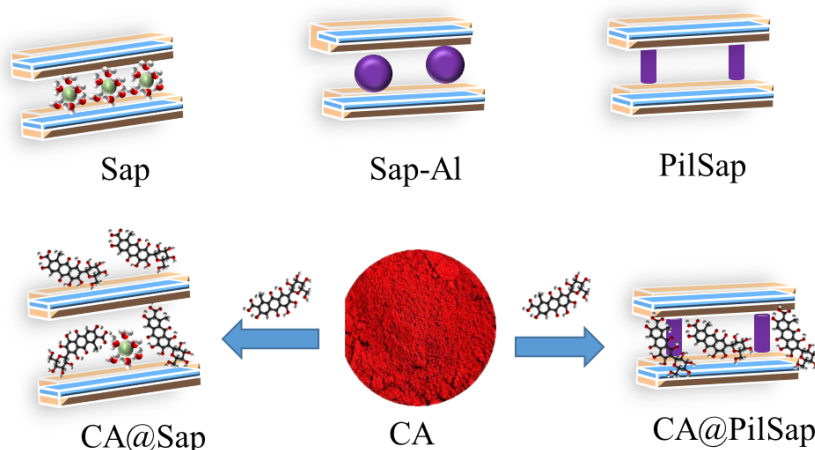


Figure 6. Scheme for formation of the CA@Sap and CA@PilSap pigments.

Although the clay minerals were not obtained, the presence of metal oxides in the hydrogel can promote the same kind of interactions with the dye, as observed in CA@PilSap (Figure 7). However, an important point should be underlined. The synthesis of the clay minerals was at pH values between 4 and 5 and under these conditions part of the carminic acid molecules

are in their mono-anionic forms ($\text{pK}_{\text{a}2} = 5.4$), which explain the partial desorption of the samples without coating, when in contact with water [4].

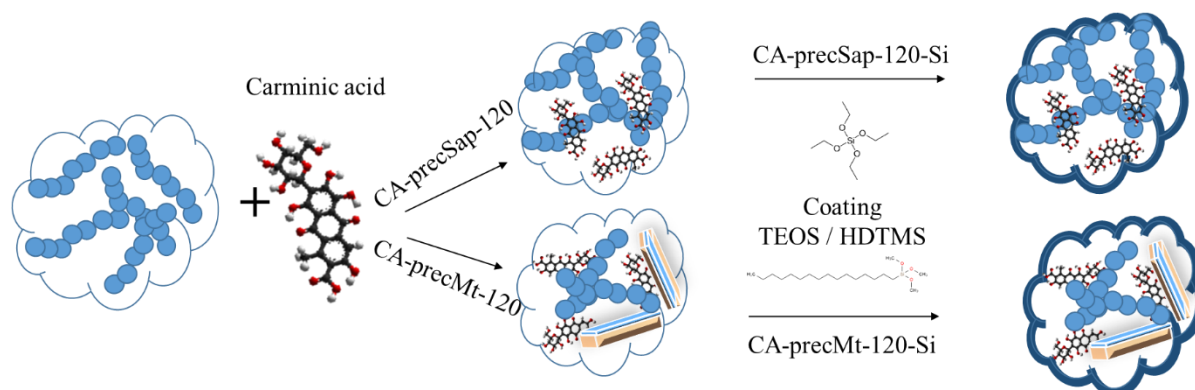


Figure 7- Scheme for the formation of coprecipitated and coated TEOS/HDTMS pigments

4.10 Color and hue variation of the hybrid pigments and photostability tests

UV-Vis spectrum of carminic acid showed a wide absorption range centered at 476 nm in the visible region attributed to $n \rightarrow \pi^*$ transitions related to the chromaticity in the dye molecule [39]. Figure SM4i showed significant blue shift (530 nm) in the Sap and PilSap samples, compared to the one observed in isolated carminic acid. It has been suggested that the p-electrons of the dye can interact with the hybridized orbitals of the oxygen atoms at the surface of the clay, leading to a stabilization of the π^* orbitals and destabilization of the π -orbitals, giving rise to a red shift of the absorption band of the adsorbed CA molecules [56,57].

CA@PilSap hybrid showed a slight decrease in the intensity and the band shifted to 541 nm. In contrast, CA@Sap showed the disappearance of the carminic acid band after irradiation (Figure 8a). The hybrid pigments prepared by coprecipitation presented similar profiles. Both spectra exhibited a wide band centered at 516 nm for CA-precSap-120 and CA-precSap-120-Si and 522 nm for CA-precMt-120 and CA-precMt-120-Si (Figure SM4iii). The differences observed for solid pigments after light exposure is probably due to the degradation/fading of the dye. Furthermore, the low photostability of CA@Sap compared to CA@PilSap suggested

weak interactions between the dye and the inorganic matrix as also attested by the release of the dye in the desorption experiments [6,16].

Photostability is an important parameter to evaluate pigments. Thus, the prepared pigments were evaluated face to visible light exposure with illuminance capacity of 66 klx for 354 h. These conditions are equivalent to approximately 39 years under normal illumination exposure for oil paintings in a museum (200 Lux; 10 h of light exposure per day; 6 days per week; 50 weeks per year) [6,19,58,59]. The measurement over CIE L^* , a^* and b^* scales notice a quantitative change over the pigments. ΔE^* variation values are due to the change of pigment structure after light exposure [6]. Color and hue variation of the hybrids obtained from these parameters for both unaged and aged pigments are presented in Figure 8-ab.

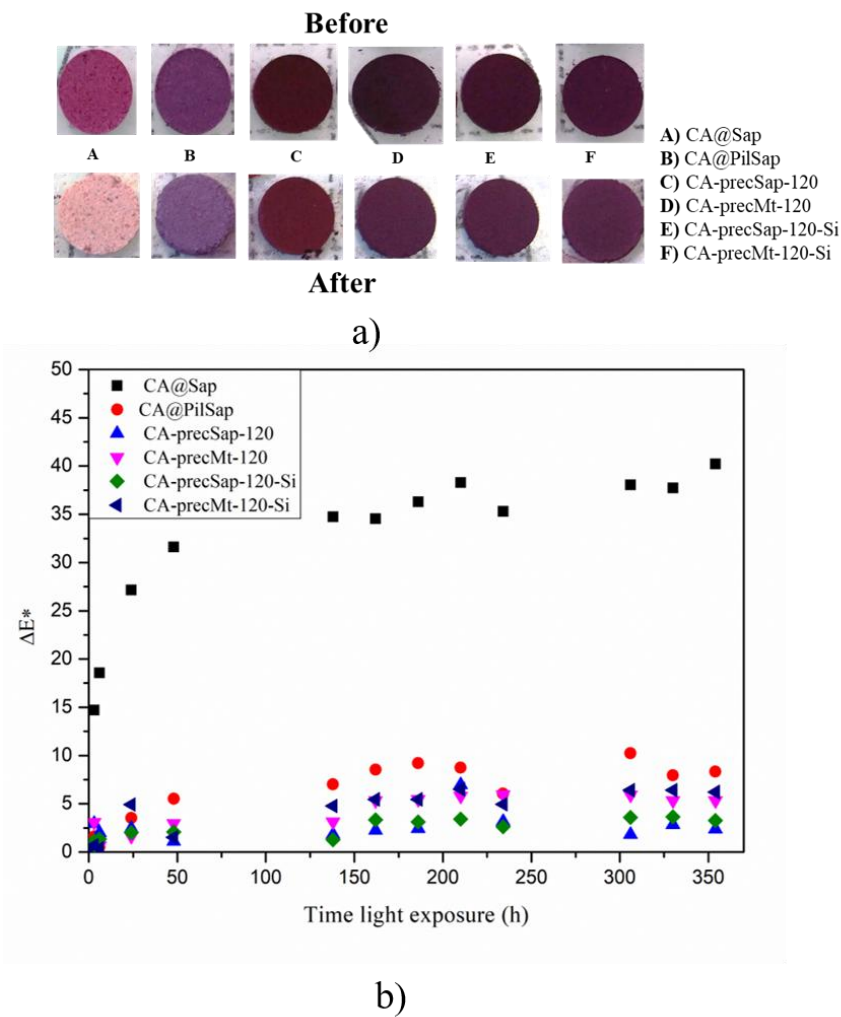


Figure 8- a) Solid pigments and b) color differences (ΔE^*) between samples before and after light exposure for 354 h with 66 klx of illumination intensity.

ΔE^* values provide information on pigment stability once the higher values demonstrate lower stability [60]. Thus, from the data the dye presented higher values of ΔE^* (more than 30) when adsorbed on saponite. In contrast, all hybrid pigments formed from pillarization or coprecipitation presented high stability with ΔE^* values lower than 10. Al-pillared based pigments were more stable than other polycations (e.g., Ti-pillared) [6]. Moreover, ΔE^* values for Al-pillared saponite were lower than ones for Al-pillared montmorillonite pigments ($\Delta E^* \sim 14$) [6,16].

Hybrid pigments formed from coprecipitation presented high stability with ΔE^* values lower than 7. In the first 138 h of exposure, both samples (CA-precSap-120-Si and CA-precMt-120-Si) presented lower ΔE^* values than those obtained for uncoated samples. These results suggested a higher stability for the coated samples. Indeed, coating the surface of the pigment disturbs the reactions with oxygen. [6,61]. TEOS / HDTMS coating acts as an inhibitor in the formation of the radicals by the formation of a protective layer. The similar effect can also occur for the dye molecules intercalated in the interlayer space of clay mineral.

5. Conclusions

Preparation of hybrid pigments through different methodologies resulted in new solids with improved properties compared with raw materials. XRD results suggested the intercalation of CA in the interlayer space of saponite in CA@SAP samples. CA desorption in both CA@PilSap and CA@Sap samples in water or alcohol was not observed. Regarding the samples produced by hydrothermal synthesis from saponite and montmorillonite precursor

gels, the XRD and TEM showed that the clay minerals were not formed, however, it was possible to observe in CA-precMt-120 micrograph the presence of some layered structures. In general, the CA adsorption in raw saponite did not generate stable hybrid pigments. In contrast, pillarization provided stronger interactions between the inorganic matrix and the dye, and resulted in more stable pigments. The "encapsulation" of the dye in saponite and montmorillonite precursor hydrogels seemed to be effective for the photostability concern, generating pigments highly stable to light exposure. Moreover, pigment coating was effective, also providing an increase in the stability of the prepared pigments.

Acknowledgements

We acknowledge the financial support from the CAPES/COFEBUB (Project n° 835/15). The authors thank the Île-de-France region and CNRS for funding.

References

- [1] Donkin RA. The Insect Dyes of Western and West-Central Asia. *Anthropos* 1977;72:847–80.
- [2] Rasmussen SA, Kongstad KT, Khorsand-Jamal P, Kannangara RM, Nafisi M, Van Dam A, et al. On the biosynthetic origin of carminic acid. *Insect Biochem Mol Biol* 2018;96:51–61. doi:10.1016/j.ibmb.2018.03.002.
- [3] Dapson RW. The history, chemistry and modes of action of carmine and related dyes. *Biotech Histochem* 2007;82:173–87. doi:10.1080/10520290701704188.
- [4] Fournier F, de Viguerie L, Balme S, Janot JM, Walter P, Jaber M.

Physico-chemical characterization of lake pigments based on montmorillonite and carminic acid. *Appl Clay Sci* 2016;130:12–7. doi:10.1016/j.clay.2016.01.046.

- [5] Rader Bowers LM, Schmidtke Sobeck SJ. Impact of medium and ambient environment on the photodegradation of carmine in solution and paints. *Dye Pigment* 2016;127:18–24. doi:10.1016/j.dyepig.2015.12.012.

- [6] Trigueiro P, Pereira FAR, Guillermin D, Rigaud B, Balme S, Janot J-M, et al. When anthraquinone dyes meet pillared montmorillonite: Stability or fading upon exposure to light? *Dye Pigment* 2018;159:384–94. doi:10.1016/j.dyepig.2018.06.046.

- [7] Chen H, Zhang Z, Zhuang G, Jiang R. A new method to prepare ‘Maya red’ pigment from sepiolite and Basic red 46. *Appl Clay Sci* 2019;174:38–46. doi:10.1016/j.clay.2019.03.023.

- [8] Zhang Y, Zhang J, Wang A. From Maya blue to biomimetic pigments: Durable biomimetic pigments with self-cleaning property. *J Mater Chem A* 2016;4:901–7. doi:10.1039/c5ta09300g.

- [9] Sánchez del Río M, Martinetto P, Reyes-Valerio C, Dooryhée E, Suárez M. Synthesis and acid resistance of Maya blue pigment. *Archaeometry* 2006;48:115–30. doi:10.1111/j.1475-4754.2006.00246.x.

- [10] Brigatti MF, Galán E, Theng BKG. Structure and Mineralogy of Clay Minerals. vol. 5. 2013. doi:10.1016/B978-0-08-098258-8.00002-X.

- [11] Kausar A, Iqbal M, Javed A, Aftab K, Nazli Z i. H, Bhatti HN, et al.

Dyes adsorption using clay and modified clay: A review. *J Mol Liq* 2018;256:395–407. doi:10.1016/j.molliq.2018.02.034.

[12] Espantaleón AG, Nieto JA, Fernández M, Marsal A. Use of activated clays in the removal of dyes and surfactants from tannery waste waters. *Appl Clay Sci* 2003;24:105–10. doi:10.1016/S0169-1317(03)00153-4.

[13] Adeyemo AA, Adeoye IO, Bello OS. Adsorption of dyes using different types of clay: a review. *Appl Water Sci* 2017;7:543–68. doi:10.1007/s13201-015-0322-y.

[14] Tangaraj V, Janot JM, Jaber M, Bechelany M, Balme S. Adsorption and photophysical properties of fluorescent dyes over montmorillonite and saponite modified by surfactant. *Chemosphere* 2017;184:1355–61. doi:10.1016/j.chemosphere.2017.06.126.

[15] Clécio L, Lima B, Castro-silva F, Silva-filho EC. Saponite-anthocyanin pigments: slipping between the sheets. *Microporous Mesoporous Mater* 2020;110148. doi:10.1016/j.micromeso.2020.110148.

[16] Guillermin D, Debroise T, Trigueiro P, de Viguerie L, Rigaud B, Morlet-Savary F, et al. New pigments based on carminic acid and smectites: A molecular investigation. *Dye Pigment* 2019;160:971–82. doi:10.1016/j.dyepig.2018.07.021.

[17] Silva GTM, Silva CP, Gehlen MH, Oake J, Bohne C, Quina FH. Organic/inorganic hybrid pigments from flavylum cations and palygorskite. *Appl Clay Sci* 2018;162:478–86. doi:10.1016/j.clay.2018.07.002.

- [18] Tian G, Wang W, Mu B, Wang Q, Wang A. Cost-efficient, vivid and stable red hybrid pigments derived from naturally available sepiolite and halloysite. *Ceram Int* 2017;43:1862–9. doi:10.1016/j.ceramint.2016.10.145.
- [19] Zhuang G, Rodrigues F, Zhang Z, Fonseca MG, Walter P, Jaber M. Dressing protective clothing: stabilizing alizarin/halloysite hybrid pigment and beyond. *Dye Pigment* 2019;166:32–41. doi:10.1016/j.dyepig.2019.03.006.
- [20] Teepakakorn AP, Bureekaew S, Ogawa M. Adsorption-Induced Dye Stability of Cationic Dyes on Clay Nanosheets. *Langmuir* 2018;34:14069–75. doi:10.1021/acs.langmuir.8b02978.
- [21] Saavedra-Labastida E, Díaz-Nava MC, Illescas J, Muro C. Comparison of the Removal of an Anionic Dye from Aqueous Solutions by Adsorption with Organically Modified Clays and their Composites. *Water Air Soil Pollut* 2019;230. doi:10.1007/s11270-019-4131-z.
- [22] Ngulube T, Gumbo JR, Masindi V, Maity A. An update on synthetic dyes adsorption onto clay based minerals: A state-of-art review. *J Environ Manage* 2017;191:35–57. doi:10.1016/j.jenvman.2016.12.031.
- [23] Bertuoli PT, Piazza D, Scienza LC, Zattera AJ. Preparation and characterization of montmorillonite modified with 3-aminopropyltriethoxysilane. *Appl Clay Sci* 2014;87:46–51. doi:10.1016/j.clay.2013.11.020.
- [24] Švara Fabjan E, Otoničar M, Gabersček M, Sever Škapin A. Surface

protection of an organic pigment based on a modification using a mixed-micelle system. *Dye Pigment* 2016;127:100–9. doi:10.1016/j.dyepig.2015.12.016.

[25] A.R. Pereira F, S. Sousa K, R.S. Cavalcanti G, B. França D, N.F. Queiroga L, Santos I, et al. Green biosorbents based on chitosan-montmorillonite beads for anionic dye removal. vol. 5. 2017. doi:10.1016/j.jece.2017.06.032.

[26] Brito DF, Da Silva Filho EC, Fonseca MG, Jaber M. Organophilic bentonites obtained by microwave heating as adsorbents for anionic dyes. *J Environ Chem Eng* 2018;6:7080–90. doi:10.1016/j.jece.2018.11.006.

[27] Bertella F, Pergher SBC. Pillaring of bentonite clay with Al and Co. *Microporous Mesoporous Mater* 2015;201:116–23. doi:10.1016/j.micromeso.2014.09.013.

[28] Queiroga LNF, Pereira MBB, Silva LS, Silva Filho EC, Santos IMG, Fonseca MG, et al. Microwave bentonite silylation for dye removal: Influence of the solvent. *Appl Clay Sci* 2019;168:478–87. doi:10.1016/j.clay.2018.11.027.

[29] Dong J, Wang Q, Zhang Y, Zhu Z, Xu X, Zhang J, et al. Colorful superamphiphobic coatings with low sliding angles and high durability based on natural nanorods. *ACS Appl Mater Interfaces* 2017;9:1941–52. doi:10.1021/acsami.6b13539.

[30] Jaber M, Brendlé J. Influence du milieu de synthèse sur la cristallisation de saponite: proposition de mécanisme réactionnel en milieux acide et basique. vol. 8. *Comptes*. 2005.

doi:10.1016/j.crci.2004.10.025.

- [31] Bergaoui L, Lambert JF, Suquet H, Che M. CuII on Al13-pillared saponites: Macroscopic adsorption measurements and EPR spectra. *J Phys Chem* 1995;99:2155–61. doi:10.1021/j100007a054.
- [32] Latthe SS, Hirashima H, Rao AV. TEOS based water repellent silica films obtained by a co-precursor sol-gel method. *Smart Mater Struct* 2009;18. doi:10.1088/0964-1726/18/9/095017.
- [33] Bisio C, Gatti G, Boccaleri E, Marchese L, Superti GB, Pastore HO, et al. Understanding physico-chemical properties of saponite synthetic clays. *Microporous Mesoporous Mater* 2008;107:90–101. doi:10.1016/j.micromeso.2007.05.038.
- [34] Jaber M, Miéché-Brendlé J. Influence du milieu de synthèse sur la cristallisation de saponite: Proposition de mécanisme réactionnel en milieux acide et basique. *Comptes Rendus Chim* 2005;8:229–34. doi:10.1016/j.crci.2004.10.025.
- [35] Prieto O, Vicente MA, Angel Bañares-Muñoz M. Study of the Porous Solids Obtained by Acid Treatment of a High Surface Area Saponite. vol. 6. 1999. doi:10.1023/A:1009657312123.
- [36] Tangaraj V, Janot J-M, Jaber M, Bechelany M, Balme S. Adsorption and photophysical properties of fluorescent dyes over montmorillonite and saponite modified by surfactant. *Chemosphere* 2017;184:1355–61. doi:10.1016/j.chemosphere.2017.06.126.
- [37] Bergaya F, Theng BKG, Lagaly G. Pillared Clays and Clay Minerals. vol. 5. 2nd ed. Elsevier Ltd.; 2013. doi:10.1016/B978-0-08-098258-8.09992-2.

- 698 [38] Figueras F. Pillared Clays as Catalysts. *Catal Rev* 1988;30:457–99.
699 doi:10.1080/01614948808080811.
- 700 [39] Munir S, Shah SM, Hussain H, Siddiq M. Adsorption of porphyrin
701 and carminic acid on TiO₂ nanoparticles: A photo-active nano-
702 hybrid material for hybrid bulk heterojunction solar cells. *J*
703 *Photochem Photobiol B Biol* 2015;153:397–404.
704 doi:10.1016/j.jphotobiol.2015.10.029.
- 705 [40] Pérez E, Ibarra IA, Guzmán A, Lima E. Hybrid pigments resulting
706 from several guest dyes onto γ -alumina host: A spectroscopic
707 analysis. *Spectrochim Acta - Part A Mol Biomol Spectrosc*
708 2017;172:174–81. doi:10.1016/j.saa.2016.04.017.
- 709 [41] Tao Q, Fang Y, Li T, Zhang D, Chen M, Ji S, et al. Silylation of
710 saponite with 3-aminopropyltriethoxysilane. *Appl Clay Sci*
711 2016;132–133:133–9. doi:10.1016/j.clay.2016.05.026.
- 712 [42] S. Petit and J. Madejova. *Fourier Transform Infrared Spectroscopy*.
713 vol. 5. 2nd ed. Elsevier Ltd.; 2013. doi:10.1007/978-3-642-74065-
714 7_7.
- 715 [43] Wang W, Kang Y, Wang A. Synthesis, characterization and
716 swelling properties of guar gum-g-poly(sodium acrylate-co-
717 styrene)/muscovite superabsorbent composites. *Sci Technol Adv*
718 *Mater* 2010;11:25006. doi:10.1088/1468-6996/11/2/025006.
- 719 [44] Földvári M. Handbook of the thermogravimetric system of minerals
720 and its use in geological practice. vol. 56. 2011.
721 doi:10.1556/CEuGeol.56.2013.4.6.
- 722 [45] Marzec A, Szadkowski B, Rogowski J, Maniukiewicz W,

- Kozanecki M, Moszyński D, et al. Characterization and properties of new color-tunable hybrid pigments based on layered double hydroxides (LDH) and 1,2-dihydroxyanthraquinone dye. *J Ind Eng Chem* 2019;70:427–38. doi:10.1016/j.jiec.2018.11.005.
- [46] Gil A, Korili SA, Trujillano R, Vicente MA. A review on characterization of pillared clays by specific techniques. *Appl Clay Sci* 2011;53:97–105. doi:10.1016/j.clay.2010.09.018.
- [47] Bergaoui L, Mrad I, Lambert J-F, Ghorbel A. A Comparative Study of the Acidity toward the Aqueous Phase and Adsorptive Properties of Al₁₃-Pillared Montmorillonite and Al₁₃-Pillared Saponite. *J Phys Chem B* 2002;103:2897–902. doi:10.1021/jp984011e.
- [48] Furrer G, Ludwig C, Schindler PW. On the chemistry of the Keggin Al₁₃ polymer. I. Acid-base properties. *J Colloid Interface Sci* 1992;149:56–67. doi:10.1016/0021-9797(92)90391-X.
- [49] Kooli F, Jones W. Systematic Comparison of a Saponite Clay Pillared with Al and Zr Metal Oxides. *Chem Mater* 1997;9:2913–20. doi:10.1021/cm970254s.
- [50] Pérez-Ramírez E, Lima E, Guzmán A. Natural betalains supported on γ -alumina: A wide family of stable pigments. *Dye Pigment* 2015;120:161–8. doi:10.1016/j.dyepig.2015.03.040.
- [51] Pérez E, Ibarra IA, Guzmán A, Lima E. Hybrid pigments resulting from several guest dyes onto γ -alumina host: A spectroscopic analysis. *Spectrochim Acta - Part A Mol Biomol Spectrosc* 2017;172:174–81. doi:10.1016/j.saa.2016.04.017.
- [52] Zhang D, Zhou CH, Lin CX, Tong DS, Yu WH. Synthesis of clay

748 minerals. Appl Clay Sci 2010;50:1–11.
 749 doi:10.1016/j.clay.2010.06.019.

750 [53] Gao K, Chang Q, Wang B, Zhou N, Qing T. Synthetic magnesium
 751 silicate hydroxide nanoparticles coated with carbonaceous shell in
 752 subcritical water condition. Appl Surf Sci 2018;450:312–7.
 753 doi:10.1016/j.apsusc.2018.04.139.

754 [54] Rasimas JP, Blanchard GJ. A study of the fluorescence and
 755 reorientation dynamics of carminic acid in primary alcohols. J Phys
 756 Chem 1995;99:11333–8. doi:10.1021/j100029a006.

757 [55] Akyuz S, Akyuz T. FT-IR and FT-Raman spectroscopic studies of
 758 adsorption of isoniazid by montmorillonite and saponite. Vib
 759 Spectrosc 2008;48:229–32. doi:10.1016/j.vibspec.2008.02.019.

760 [56] Schoonheydt R, Johnston C. Surface and interface chemistry of clay
 761 minerals. vol. 1. 2nd ed. Elsevier Ltd.; 2013. doi:10.1016/S1572-
 762 4352(05)01003-2.

763 [57] Gonçalves JLS, Valandro SR, Poli AL, Schmitt CC. Influence of
 764 clay minerals on curcumin properties: Stability and singlet oxygen
 765 generation. J Mol Struct 2017;1143:1–7.
 766 doi:10.1016/j.molstruc.2017.04.073.

767 [58] Zhuang G, Jaber M, Rodrigues F, Rigaud B, Walter P, Zhang Z. A
 768 new durable pigment with hydrophobic surface based on natural
 769 nanotubes and indigo: Interactions and stability. J Colloid Interface
 770 Sci 2019;552:204–17. doi:10.1016/j.jcis.2019.04.072.

771 [59] De Queiroga LNF, França DB, Rodrigues F, Santos IMG, Fonseca
 772 MG, Jaber M. Functionalized bentonites for dye adsorption:

Depollution and production of new pigments. J Environ Chem Eng
2019;7:103333. doi:10.1016/j.jece.2019.103333.

[60] Kokalj D, Zlatić E, Cigić B, Vidrih R. Postharvest light-emitting
diode irradiation of sweet cherries (*Prunus avium* L.) promotes
accumulation of anthocyanins. Postharvest Biol Technol
2019;148:192–9. doi:10.1016/j.postharvbio.2018.11.011.

[61] Lencione D, Gehlen MH, Trujillo LN, Leitao RCF, Albuquerque
RQ. The spatial distribution of the photostability of thionine in
zeolite L nanochannels investigated by Photobleaching Lifetime
Imaging Microscopy. Photochem Photobiol Sci 2016;15:398–404.
doi:10.1039/c5pp00418g.